Three-Dimensional Structure of Kynureninase from *Pseudomonas fluorescens*[†,‡]

Cory Momany,[§] Vladimir Levdikov,[§,||] Lena Blagova,[§,||] Santiago Lima,[⊥] and Robert S. Phillips*[,||,⊥]

Departments of Chemistry and of Biochemistry and Molecular Biology, University of Georgia, and Department of Pharmaceutical and Biomedical Sciences, College of Pharmacy, University of Georgia, Athens, Georgia 30602

Received September 26, 2003; Revised Manuscript Received December 5, 2003

ABSTRACT: Kynureninase [E.C. 3.7.1.3] is a pyridoxal-5′-phosphate (PLP)-dependent enzyme that catalyzes the hydrolytic cleavage of L-kynurenine to anthranilic acid and L-alanine. Sequence alignment with other PLP-dependent enzymes indicated that kynureninase is in subgroup IVa of the aminotransferases, along with nifS, CsdB, and serine-pyruvate aminotransferase, which suggests that kynureninase has an aminotransferase fold. Crystals of *Pseudomonas fluorescens* kynureninase were obtained, and the structure was solved by molecular replacement using the CsdB coordinates combined with multiple isomorphous heavy atom replacement. The coordinates were deposited in the PDB (ID code **1QZ9**). The structure, refined to an *R* factor of 15.5% to 1.85 Å resolution, is dimeric and has the aminotransferase fold. The structure also confirms the prediction from sequence alignment that Lys-227 is the PLP-binding residue in *P. fluorescens* kynureninase. The conserved Asp-201, expected for an aminotransferase fold, is located near the PLP nitrogen, but Asp-132 is also strictly conserved and at a similar distance from the pyridinium nitrogen. Mutagenesis of both conserved aspartic acids shows that both contribute equally to PLP binding, but Asp-201 has a greater role in catalysis. The structure shows that Tyr-226 donates a hydrogen bond to the phosphate of PLP. Unusual among PLP-dependent enzymes, Trp-256, which is also strictly conserved in kynureninases from bacteria to humans, donates a hydrogen bond to the phosphate through the indole N1-hydrogen.

Kynureninase [E.C. 3.7.1.3] is a pyridoxal-5′-phosphate (PLP[1])-dependent enzyme that catalyzes the hydrolytic cleavage of L-kynurenine to anthranilic acid and L-alanine (eq 1). This reaction is a key step in the catabolism of

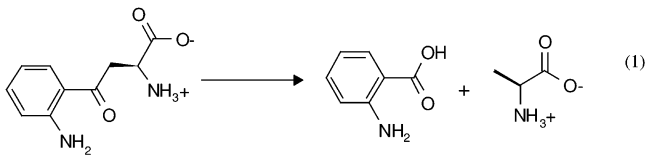

(1)

L-tryptophan by *Pseudomonas fluorescens* and some other bacteria (*1*). In fungi and vertebrates, kynurenine is first hydroxylated to 3-hydroxykynurenine, which is the preferred substrate of kynureninase in those organisms, resulting in 3-hydroxyanthranilate and L-alanine.

Kynureninase also plays a role in the biosynthesis of NAD(P)$^+$. The product of kynureninase, 3-hydroxyanthranilate, is subsequently converted by 3-hydroxyanthranilate-3,4-dioxygenase to quinolinic acid, which is a precursor of NAD(P)$^+$. However, quinolinic acid is also a neurotoxin, due to its agonist effects on the *N*-methyl-D-aspartate (NMDA) receptor (*2*). Excessive levels of quinolinic acid have been implicated in the etiology of a wide range of neurological disorders, such as epilepsy, stroke, and AIDS-related dementia (*3*−*10*). Thus, inhibitors of kynureninase are of interest as potential drugs for the treatment of these CNS disorders.

The kynureninase from *P. fluorescens*, a dimer with a subunit molecular weight of 45000, has been cloned and expressed in *Escherichia coli* (*11*). The *P. fluorescens* kynureninase is highly homologous to the human enzyme, with 28% identical residues (*11*). Thus, the three-dimensional structures must be similar. Sequence alignment with other PLP-dependent enzymes shows that kynureninases are in subgroup IVa of the aminotransferases, along with nifS, CsdB, and serine-pyruvate aminotransferase, suggesting that kynureninase has an aminotransferase fold (*12*). In the present work, we obtained crystals of *P. fluorescens* kynureninase suitable for X-ray diffraction and solved the structure to 1.85 Å. The structure confirms the prediction that kynureninase has the aminotransferase fold. Furthermore, the structure shows several unusual features, including two conserved aspartate residues in the PLP-binding site, Asp-201 and Asp-132, and a conserved tryptophan, Trp-256, which donates a hydrogen bond to the phosphate of PLP. The implications of the structure for the mechanism of kynureninase are discussed. Furthermore, the structure of the bacterial kynureninase will help in the structure determination

[†] This research was partially supported by grants from NSF-NATO (DGE-97-10853) to V.L. and NIH (GM42588-13) to R.S.P.

[‡] Coordinates are deposited in the Protein Data Bank as ID code **1QZ9**.

* To whom correspondence should be addressed.. Phone: (706) 542-1996. Fax: (706) 542-9454. E-mail: rsphillips@chem.uga.edu.

[§] Department of Pharmaceutical and Biomedical Sciences, College of Pharmacy.

[||] Department of Chemistry.

[⊥] Department of Biochemistry and Molecular Biology.

[1] Abbreviations: BME, 2-mercaptoethanol; DTT, dithiothreitol; IPTG, isopropyl β-D-thiogalactopyranoside; MIR, multiple isomorphous replacement; MR, molecular replacement; PLP, pyridoxal-5′-phosphate; PMP, pyridoxamine-5′-phosphate; PMSF, phenylmethylsulfonyl fluoride; TCEP, tris(2-carboxyethyl)phosphine hydrochloride.

10.1021/bi035744e CCC: $27.50
Published on Web 01/16/2004

Scheme 1: Proposed Reaction Mechanism of Kynureninase

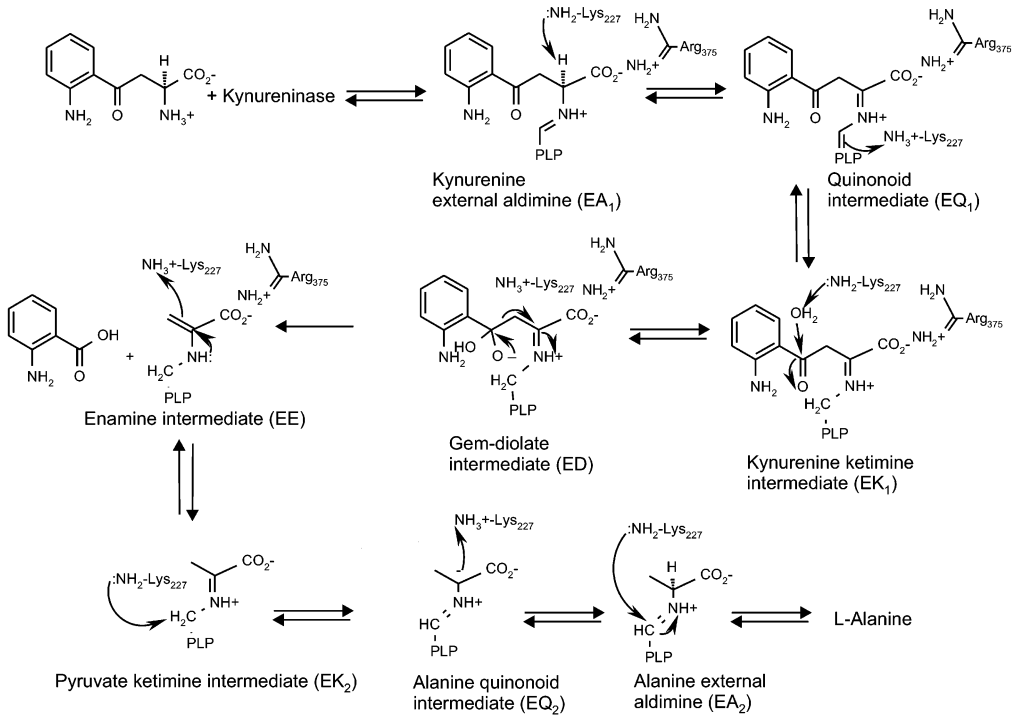

of the human kynureninase, which in turn would be valuable for the design and evaluation of novel, selective, and more potent inhibitors.

MATERIALS AND METHODS

Cloning, Expression, and Purification. Recombinant kynureninase was purified initially from *E.coli* cells containing plasmid pTZ18U with the gene coding for *P. fluorescens* kynureninase (*11*). To prepare an expression construct amenable for selenomethionine substitution, pTZ18U was used to subclone the kynureninase gene into pSapKO-WT, a modified pET28b vector (Novagen) containing *Sap*I sites introduced between the *Eco*RI and *Nco*I sites of the original vector (*13*). This construct, pLB1kyn, was transformed into the methionine auxotroph *E. coli* B834 (DE3).

Alternative purification schemes were developed after difficulties were encountered in producing crystals using the original protocol (*11*). *E. coli* cells containing pTZ18U or pLB1kyn were grown for 15−17 h at 37 °C in 50 mL inoculums of LB medium (1% tryptone, 0.5% yeast extract, 0.5% sodium chloride; the pH was adjusted to 7.0 with sodium hydroxide) containing 100 μg/mL carbenicillin. After inoculation into 1 L of the same medium, cells were grown for 4−5 h before induction by 1 mM IPTG. The cells were collected by centrifugation at 4 °C for 15 min at 10000*g* and suspended in 30 mL of buffer (5 mM potassium phosphate, pH 8.0, containing 0.2 mM PLP). A 1 mM concentration of PMSF (1 M stock in 2-propanol) was added to the cell suspension. After sonication on ice for 3 min in 1 min increments with a Fisher Scientific 550 sonic dismembrator, cell debris was removed by centrifugation for 30 min at 25000*g* at 4 °C. A solution of 2% (w/v) protamine sulfate (4 mL) was added dropwise to the supernatant, and the precipitant was separated by centrifugation at 4 °C for 20 min at 55000*g*. The subsequent purification steps were carried out by two procedures, either of which were able to produce homogeneous enzyme that crystallized.

Purification scheme 1 continued by loading the enzyme onto a HiTrap Q (Amersham-Pharmacia, 5 mL) column equilibrated with 5 mM potassium phosphate buffer, pH 8.0, at a flow rate of 5 mL/min, washing with the same buffer, and then eluting using a 0−0.5 M NaCl (same buffer) gradient over 20 column volumes. The active fractions were combined, and the solution was replaced by 5 mM potassium phosphate and 0.2 mM PLP buffer by repeated (two times) concentration (5 mL) and dilution (50 mL) with 5 mM potassium phosphate buffer containing 0.2 mM PLP using a YM 30 ultrafiltration membrane (Amicon). The enzyme was applied to an ω-aminohexylagarose (Sigma) column equilibrated with 5 mM potassium phosphate buffer, pH 8.0, washed with the same buffer, and eluted using a 0−0.5 M NaCl gradient over 20 column volumes. After a buffer change to 5 mM potassium phosphate containing 0.2 mM PLP by ultrafiltration as before, the sample was applied to a second HiTrap Q column equilibrated with 5 mM potassium phosphate buffer, pH 8.0. The enzyme was washed with the same buffer and then eluted using a 0−0.5 M NaCl gradient. The buffer was changed to 0.5 M potassium phosphate containing 0.2 mM PLP by ultrafiltration. The resulting solution was then applied to a Phenyl-Sepharose (Amersham-Pharmacia) column equilibrated with 0.5 M potassium phosphate buffer, pH 8.0. The enzyme was washed with the same buffer and then eluted using a 0.5 M to 5 mM potassium phosphate buffer gradient.

The second purification scheme proved to be difficult to reproduce and involved concentration of the crude extract (30 mL) to 3 mL on a YM 30 ultrafiltration membrane (Amicon) and subsequent dilution to 15 mL with water containing 0.2 mM PLP. The diluted protein was applied to a hydroxyapatite column (BioRad, 3.0 cm × 15 cm) equilibrated with 1 mM potassium phosphate buffer, pH 8.0, washed with the same buffer, and then eluted with 5 mM potassium phosphate, pH 8.0. The active fractions from either

Table 1: Data Collection, Scaling, and Phasing Statistics

data set	resolution, Å	$R_{merge}(I)$, %	redundancy	completeness, %	R_{cryst},[c] %	no. of heavy atom sites	phase power[d]
native	58.7−1.85	6.3	13.9	96.8			
Xe	20.0−2.6	8.7	14.6	99.9	16.3	2	0.91
TMer[a]	20.0−3.0	7.8	3.4	98.6	35.2	3	1.14
PTCP[b]	20.0−3.4	8.4	5.7	87.6	26.9	1	0.41
PTCP[b]	20.0−3.4	7.0	4.1	98.1	12.0	1	0.45
NaBr	20.0−2.6	6.6	6.8	99.8	16.0	12	0.89

[a] tMer = thiomersalyl ($C_9H_9HgNa_2O_2S$). [b] PTCP = potassium tetrachloroplatinate(II). [c] R_{cryst} (%) $=100\sum|F_P - F_{PH}|/\sum|F_P|$, where F_P and F_{PH} are the observed structure factors for the native and heavy atom derivatives. [d] Phase power = f_h/E, where f_h is the RMS contribution of the heavy atom and E is the RMS lack of closure error.

of the above methods, containing specific activities of greater than 15, were combined and concentrated on an Amicon membrane to the final concentration of the protein equal to 40 mg/mL. The purified protein exhibited a single band on silver-stained SDS−PAGE on PhastGel Homogeneous 20 (Amersham-Pharmacia). Purified protein was usually divided into 100 μL portions and stored at −78 °C. The protein concentration was estimated by measuring the absorbance at 280 nm on a Pharmacia Biotech Ultrospec 2000 spectrophotometer using the extinction coefficient $E^{1\%}{}_{1cm} = 14.0$ (*14*). The activity of kynureninase was determined by following the decrease in absorbance at 360 nm ($\Delta\epsilon = -4500\ M^{-1}\ cm^{-1}$) as kynurenine is hydrolyzed to anthranilic acid.

Crystallization, Structure Determination, and Refinement. Crystallization experiments were performed using the hanging-drop vapor diffusion technique at room temperature (*15*, *16*) using Sparse Matrix approaches (*17*). Heavy atom derivatives of thiomersalyl ($C_9H_9HgNa_2O_2S$) and potassium tetrachloroplatinate(II) were obtained by soaking native protein crystals in solutions of heavy atom compounds in the stabilizing solution, 40% (w/v) PEG 400, 0.2 M LiCl, 0.2 mM PLP, 5 mM potassium phosphate buffer, pH 8.0, at concentrations of 2.5−4.0 mM for 1−3 days. A Xe heavy atom derivative was obtained by suspending the crystals in a Xe atmosphere for 10 min at a 700 kPa pressure using a Molecular Structure Corp. Cryo-Xe-Siter. A NaBr derivative was obtained by briefly (10−15 s) transferring the native crystals through stabilizing solution containing 1 M NaBr (*18*). X-ray diffraction data from a single crystal of native protein to 1.85 Å resolution and the five heavy atom derivatives were collected in-house using a MAR Research imaging plate scanner mounted on a Rigaku RU-200 generator (Cu Kα, $\lambda = 1.5418$ Å). All data were collected at −180 °C except the thiomersalyl derivative, which was collected at room temperature. The data were processed and merged using the programs DENZO and SCALEPACK (*19*, *20*). The statistics for data collection and processing are summarized in Table 1.

Phases for the protein structure factors at 2.6 Å resolution were derived by a combination of MIR and MR methods. Initial heavy atom positions were obtained from the program SOLVE (*21*) using the Xe derivative. A second heavy atom, on a special position, was found using Harker sections of the anomalous difference Patterson map. A molecular replacement solution was found using the Cα model of CsdB from *E. coli* (PDB code **1C0N**) (*22*, *23*). The level of sequence identity between kynureninase and CsdB is 16%. A cross-rotation function with an integration radius of 30 Å and a translation function were calculated in the resolution range from 10 to 6.5 Å using AMORE (*24*). The rotation function solution was 43rd in the solutions list. The translation solution had a correlation of 44.5 and *R* factor of 50.5%. Correlations for wrong peaks of the translation function were below 42.2. Two criteria for selection of the right solution were used. First, the solution model packed in the unit cell with formation of an appropriate biologically sensible dimer. Second, the peaks corresponding to the Xe heavy atom positions were present in the difference Fourier map for the Xe derivative calculated with MR phases. The MR phases were used to find heavy-atom-binding sites in difference Fourier syntheses for four other derivatives. The heavy atom parameters were refined jointly taking into account anomalous dispersion using the program MLPHARE (*25*) from the CCP4 suite (*26*). The MIR phases had a mean figure of merit of 0.52 at 2.6 Å resolution. Statistics for the heavy atom refinement are given in Table 1. MIR phases were improved using solvent flattening and histogram matching using the DM program (*27*) from the CCP4 suite. The quality of the map allowed us to trace above 90% of the polypeptide chain including side chains using residues conserved between CsdB and kynureninase as consistency markers. The model was built using the program O (*28*). The coordinate refinement was carried out using the stereochemically restrained maximum-likelihood method, program REFMAC, in the CCP4 package (*29*) coupled with automated building and updating of the solvent structure using ARP (*30*). The lysine was refined as an aldimine linkage with the cofactor having a target bond length of 1.450 Å and appropriate bond geometries. All X-ray data were used with no cutoff on amplitudes or resolution. In later rounds, TLS refinement was performed by dividing the protein into four domains (domain I, residues 1−35 and 299−405; domain 2, residues 36−96, 205−241, and 282−298; domain 3, residues 242−281; domain 4, residues 97−204). TLS refinement dropped the *R* factor from 17.8% to 16.1% and R_{free} from 24.3% to 20.7%, thus validating its use. Side chains for residues Gln 21, Glu 27, Arg 87, Glu 118, Gln 160, Gln 164, Gln 185, Gln 262, Glu 370, and Arg 401 were not visible in electron density maps and were not refined. The orientations of glutamine, asparagine, and histidine residues were checked, and hydrogen atoms were added by the program MOLPROBITY (*31*) before the later rounds of refinement. A continuous, nonproteinacious feature in the electron density maps was modeled as a short polyethylene glycol, although it is possibly a fatty acid on the order of myristic acid. Statistics for the final refinement round are given in Table 2.

Site-Directed Mutagenesis. Mutagenesis of *P. fluorescens* kynureninase was performed using the QuikChange kit from Stratagene. The mutagenesis primers were designed accord-

Table 2: Refinement Statistics and Figures of Quality for the Final Refined Structure

resolution range (last shell)	58.7−1.85 Å (1.90−1.85)
no. of reflns (last shell)	29707 (2078)
R factor (last shell)	0.155 (0.377)
R_{free} factor (5% of data excluded from refinement) (last shell)	0.192 (0.411)
no. of protein atoms/no. of water molecules	3158/433
ligands	Cl^- and PEG
RMS deviations from ideal geometry	
bond length	0.009 Å
bond angle	1.186°
mean *B* factor	23.48 Å^2
percentage of residues in Ramachandran plot in favored/additional/generous/disallowed regions	88.4/10.5/1.1/0

ing to the instructions obtained with the kit. All mutant kynureninases were sequenced to confirm the presence of the desired mutation and the absence of unintended mutations elsewhere. The reactions were cycled in a thermocycler as follows: 1 cycle of 30 s at 95 °C, 16 cycles of 30 s at 95 °C, 1 min at 55 °C, and 8 min at 68 °C. The mutant proteins were purified as described previously (*11*).

PLP binding measurements were performed with apoenzymes that were obtained by overnight incubation with 0.2 M L-alanine, followed by gel filtration on a PD-10 column (Amersham-Pharmacia) to remove the L-alanine and PMP. Assays were performed at 37 °C in a Molecular Devices SpectraMax340 microplate reader. Reactions contained 1−10 nM kynureninase, except in the case of D201A, where the enzyme was 1 μM. The reaction mixtures contained, in a total of 300 mL, 0.04 M potassium phosphate, pH 8, 0.2 mM L-kynurenine, and varying amounts of PLP. The reactions were followed by the decrease in absorbance at 360 nm, after a 5−10 min preincubation to allow PLP binding. The PLP activity data were fit to a Michaelis−Menten equation using the program HYPER (32) to obtain the PLP binding constant.

Sequence Analysis. A PSI-BLAST sequence analysis (*33*) was performed at the National Center for Biotechnology Information (NCBI) web server using human and *P. fluorescens* kynureninase amino acid sequences to build a profile that was then searched and redefined three times. Homologues were aligned using CLUSTAL-W (*34*) in BioEdit (Tom Hall) that had probability scores above $2e^{-33}$. Several bacterial kynureninase amino acid sequences were corrected at the N-terminus on the basis of sequence alignment and the presence of obvious Shine−Dalgarno (*35*) sequences incorrectly assigned in the protein sequence. Atrazine hydrolase appeared to be at the transition between kynureninases and nifS homologues and was not included in the alignment.

RESULTS

Purification and Crystallization of P. fluorescens Kynureninase. Because kynureninase failed to crystallize reproducibly using the previously reported purification scheme, a new approach to purify the enzyme was developed. Attempts to purify the protein using hydroxyapatite columns were difficult to reproduce, with some batches of protein yielding high-purity protein and other batches not binding to the hydroxyapatite column and thus necessitating a different strategy. The longer protocol, with multiple Q columns and the phenyl-Sepharose column, reproducibly produced protein that crystallized. The enzyme in 5 mM potassium phosphate buffer and 0.2 mM PLP, pH 8.0, loses 40% of its activity when stored at 4 °C for 1 week. We observed an almost 4-fold decrease in enzyme activity when the protein was stored at −78 °C for 3 months. The enzyme is more stable in buffer of higher ionic strength. If stored in 0.1 M phosphate buffer, it is stable toward freezing at −78 °C for at least one year. Attempts to prepare a selenomethionyl-substituted kynureninase for MAD phasing from the construct on plasmid pTZ18U proved difficult, with an unacceptably low yield. The long expression times used with this plasmid appeared to be detrimental, so the kynureninase gene was transferred to a pET28b vector (Novagen). While the structure was solved before this plasmid construct was used to prepare selenomethionyl-modified kynureninase, the yield of the enzyme was significantly improved over that of the pTZ18U construct. Thus, the pET28b-based plasmid was useful for isolation of native kynureninase.

Three distinct crystal morphologies were identified during crystallization trials. Thin, platelike yellow crystals (0.3 × 0.2 × 0.03 mm) were obtained by vapor diffusion using a mixture of lithium chloride (1.2−1.6 M) and PEG 8000 (10% w/v) as the precipitant. The protein drops contained 20−25 mg mL^{-1} kynureninase, 0.4 M lithium chloride, and 5% PEG 8000. Preliminary X-ray studies showed that these crystals had Laue symmetry *mmm* with unit cell parameters $a = 83.5$ Å, $b = 89.7$ Å, and $c = 104.2$ Å. Colorless dagger-like crystals were obtained when the drop, containing 20 mg/mL protein, 0.4 M lithium chloride, 3% (w/v) PEG 8000, and 3% (w/v) PEG 600, was equilibrated against the reservoir solution consisting of 1.2 M lithium chloride, 8% (w/v) PEG 8000, and 2% (w/v) PEG 600. These crystals were rather small and not suitable for X-ray experiments. Crystals suitable for X-ray diffraction studies were obtained when the protein (20 mg mL^{-1} in 5 mM potassium phosphate buffer and 0.2 mM PLP, pH 8.0 or 6.0) was mixed with 0.15−0.2 M (final) lithium chloride and 10% (w/v) PEG 400 or 600 and suspended over a reservoir consisting of 25−35% (w/v) PEG 400 or 600 only or with the addition of 0.15−0.4 M lithium chloride. Yellow isometric crystals appeared in 10−15 days at room temperature and grew to dimensions of 0.5 × 0.5 × 0.4 mm in approximately 1 week. Crystals grown in PEG 400 at pH 6.0 were more suitable for a structure determination both from a size standpoint and because they could be directly flash frozen with no evidence of ice crystal formation visible as a haze around the crystal or in the diffraction pattern.. Fresh crystals diffracted beyond 2.0 Å resolution, but the quality of the diffraction decreased markedly with crystal age. They belong to the $P3_121$ space group with cell dimensions $a = b = 68.08$ Å and $c = 138.98$ Å. These crystals were used for the kynureninase structure determination.

Crystals of kynureninase form readily from precipitate. The influence of reducing agents on the formation of the kynureninase crystals was studied by adding DTT, βME, and TCEP to the crystallization drops to achieve final 1−5 mM concentrations of the reductant in the hanging drops. The presence of the additives resulted in a significant decrease of amorphous precipitate from which formation of the crystals took place (data not shown), but the presence of the reductant did not improve the diffraction quality, and thus reductants were not used in further structural studies.

Overall Fold. The biologically active structure of kynureninase, like many PLP-dependent enzymes, is a homodimer (*36*). With this particular unit cell and the $P3_121$ space group, a kynureninase monomer makes up the asymmetric unit. Its 2-fold related monomer is generated by the symmetry operator ($X - Y$, $-Y$, $2/3 - Z$) translated one unit cell along the crystallographic *b* axis. Electron density is generally well ordered for residues Thr-2 to Ala-405, although a few side chains had weak density. In particular, the side chain of conserved Phe 263 was poorly ordered. The density for the PLP cofactor clearly suggests that a stable aldimine linkage between Lys-227 is present. A single tentative chloride ion in the active site was assigned on the basis of the strong electron density feature and a strong anomalous signal in the native anomalous difference Fourier map. All of the sulfur atoms, with the exception of Cys-194, have strong anomalous difference density, indicating that the data and final structure are of high quality. The crystal structure has good geometry with RMS deviations from ideal bonds lengths and angles of 0.009 Å and 1.186° (Table 2). No non-glycine residues are in the disallowed regions of the Ramachandran plots, while residues Leu60, Glu118, Gln144, and Cys280 are in the generous regions. The final *R* factor, including hydrogen atoms, was 15.5% with an R_{free} of 19.2% (5% of the data) at 1.85 Å resolution. Figure 1 illustrates the overall fold of kynureninase. Secondary structure elements identified with PROCHECK are associated with the sequence in Figure 2.

Kynureninase is structurally most similar to L-cysteine L-cystine C−S lyase (C-DES; PDB accession no. **1ELQ**) with a close second being the protein used for molecular replacement, CsdB (PDB accession no. **1C0N**) (Figure 3). The overall α-carbon RMS deviations are 2.3 and 2.8 Å over 349 and 368 residues when analyzed by DALI. Figure 3 illustrates the degree of structural similarity among kynureninase, CsdB, and C-DES. On the basis of the DALI fold match and sequence alignments (*12*), kynureninase belongs in the aminotransferase fold type I, class IVa. Like other fold type I enzymes, the monomer folds into a "large domain" (residues 34−301) consisting of a Greek-key $\alpha\beta\alpha$ fold containing a seven-stranded mixed β-pleated sheet (S3, S10, S9, S8, S6, S4, and S5) with seven flanking α-helices (H5, H10, H9, H8, H7, H6, and H12) and several short β-strands (S2, S7, S11, and S12) and outside helices (H3 and H4), all enfolding the PLP cofactor. The "small domain" (residues 302−405) is an $\alpha\beta$ fold with four antiparallel β-strands (S13, S14, S15, and S16) and three α-helices (H13, H14, and H15). Like CsdB and C-DES, there is an N-terminal extension from the large domain, helices (H1 and H2) that are associated mainly with the small domain. Lys-227 extends from a loop located between the two domains to interact with the PLP cofactor. When the domains are compared separately, the

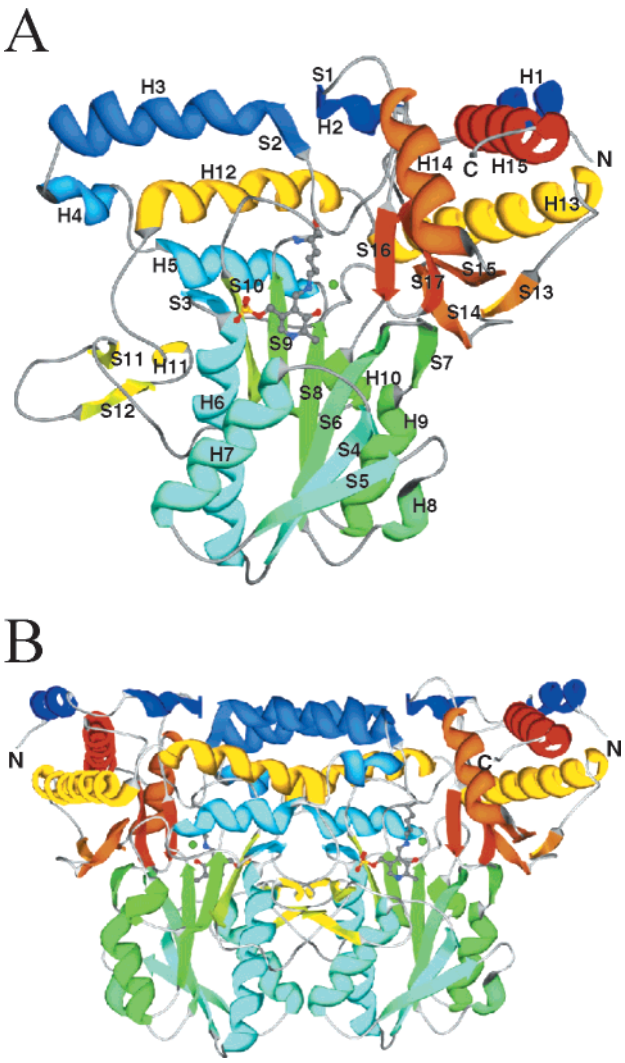

FIGURE 1: Ribbon representation of the kynureninase monomer (A) and the biologically functional dimer (B). Secondary structure assignments are color coded blue to red, amino terminus to carboxy terminus. The PLP cofactor and a chloride ion (colored green) in the active site are rendered in CPK format. The figures were generated using Swiss-PdbViewer version 6.3 (*43*) and rendered with POV-RAY (http://www.povray.org). Labels were added using Adobe Illustrator.

RMS deviations are smaller than the overall deviation. The large domains (residues 29−301) superpose with an RMS deviation of 2.2 Å with C-DES and 2.6 Å with CsdB. The small domains (residues 302−403) have RMS deviations of 1.6 Å with CsdB and 2.1 Å with C-DES. Several other PLP proteins, for instance nifS-like protein ($Z = 12.3$) and L-*allo*-threonine aldolase ($Z = 11.7$), have higher *Z*-scores for the small domain than CsdB (6.0) and C-DES (5.6).

Structure comparisons of kynureninase with CsdB and C-DES reveal several regions of structure variation. Kynureninase has an extra α-helix at the amino terminus, H1, that is not present in CsdB or C-DES (Figure 3). Some kynureninases, for instance from *Caenorhabditis elegans*, have appreciably more amino acids at the amino terminus (Figure 2). Fujii et al. identified several regions of significant structural differences between CsdB and NifS that were denoted dr-A* through dr-D (*22*). Several additional insertions and deletions with respect to C-DES and CsdB (dr-E through dr-G) are shown in Figure 3 beyond the original four identified. Region dr-A*, located between helices H3

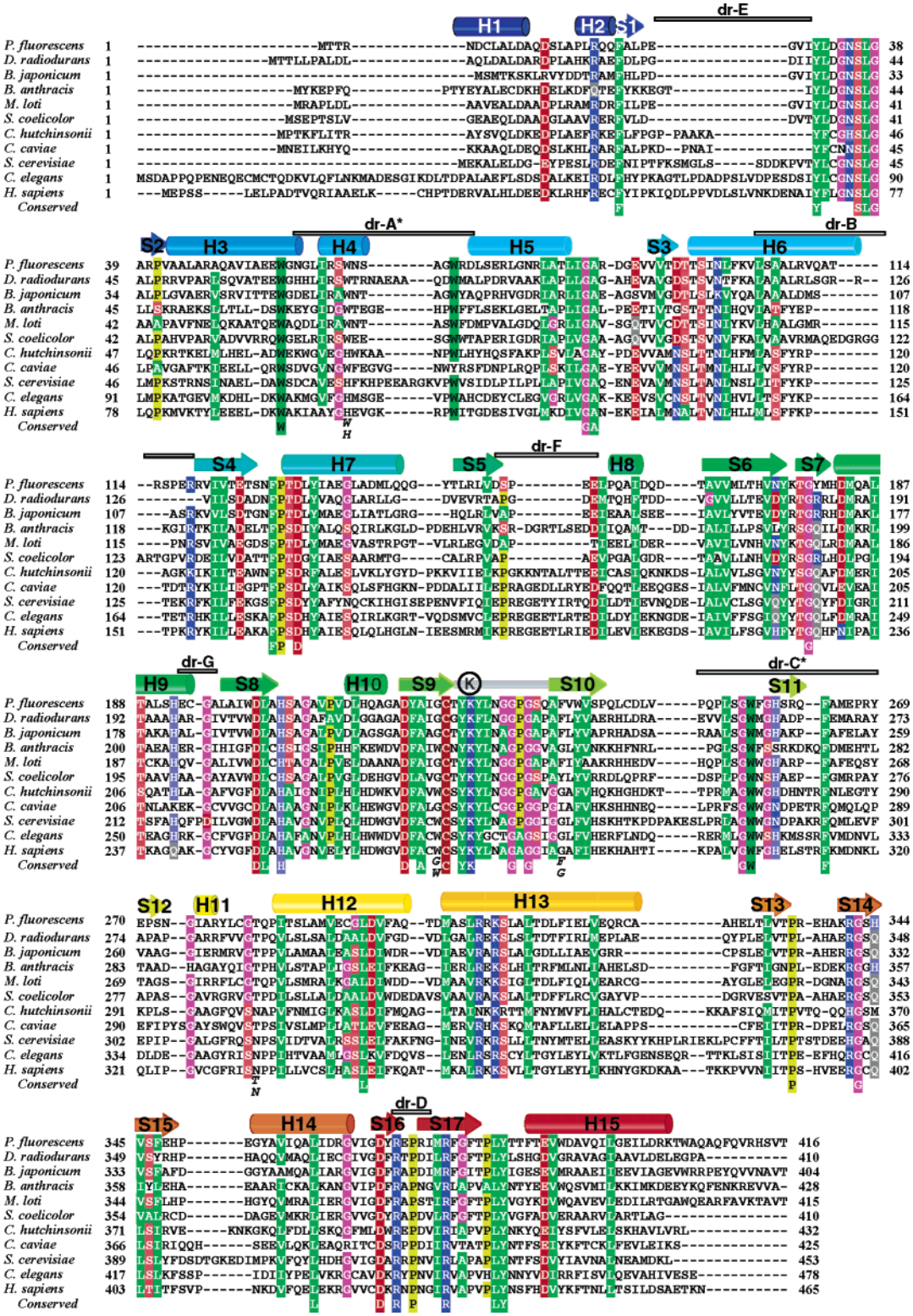

FIGURE 2: Multiple sequence alignment of kynureninases from multiple species. Only a subset of the sequences aligned is represented to save space. Helical secondary structures in the *P. fluorescens* kynureninases structure are denoted as cylinders and β-strands as extended arrows above the sequences. Colored blocks in the sequences represent regions of >80% identity with the colors dependent on the amino acid (P, yellow; G, purple; AVILYFWM, green; HKR, blue; STDE, red; NQ, gray; C, brown). Double mutations identified from the structure are shown in the conserved sequence as double letters, representing the possible amino acids at that position. The figure was generated using a CLUSTAL-W alignment (*34*) in the program BioEdit (Tom Hall). The circled letter K is Lys-227 that binds PLP. Abbreviations and NCBI accession: *P. fluorescens*, *Pseudomonas fluorescens*; *D. radiodurans*, *Deinococcus radiodurans* NP_285661 putative kynureninase; *B. japonicum*, *Bradyrhizobium japonicum* USDA 110 NP_770799; *B. anthracis*, *Bacillus anthracis* A2012 NP_656639 aminotransferase class V; *M. loti*, *Mesorhizobium loti* NP_102390 probable kynureninase; *S. coelicolor*, *Streptomyces coelicolor A3* NP_627839 putative hydrolase; *C. hutchinsonii*, *Cytophaga hutchinsonii* ZP_00118864 hypothetical protein; *C. caviae*, *Chlamydophila caviae* GPIC NP_829432; *S cerevisiae*, *Saccharomyces cerevisiae* NP_013332; *C. elegans*, *Caenorhabditis elegans* NP_509023; *H. sapiens*, *Homo sapiens* NP_003928. A more complete alignment is given in the Supporting Information. Structural differences described in the text among kynureninase, CsdB, and C-DES that show significant sequence variations within the kynureninases are denoted as dr-A through dr-G.

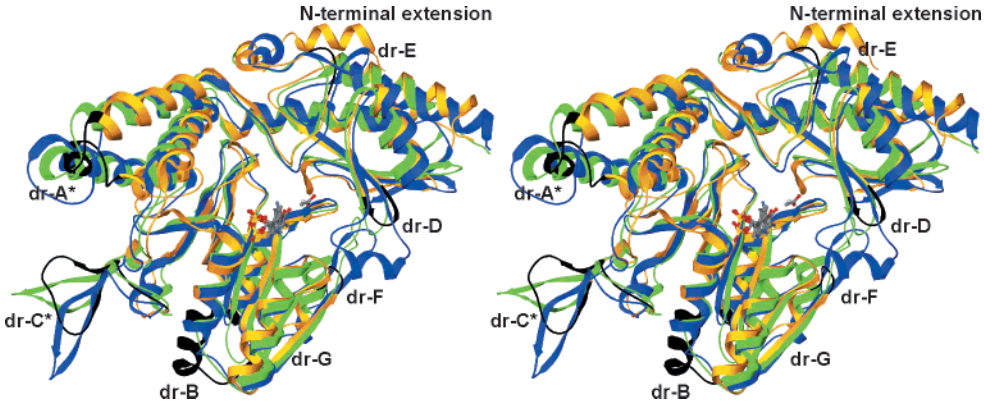

FIGURE 3: Stereo representation of superpositioned kynureninase, CsdB, and C-DES. The structures of kynureninase (colored orange), CsdB (**1C0N**, blue), and C-DES (**1ELQ**, green) were superpositioned using the "Magic Fit" and "Improve Fit" options in Swiss-PdbViewer (*43*). Labeled regions colored black in the kynureninase denote regions of significant structural variation following the scheme presented for CsdB (Figure 9 of Fujii et al. (*22*)) but extended further here, "dr-A*" for kynureninase residues Asn-58 to Asp-71 between H3 and H5, "dr-B" for residues Leu-105 to Arg-120 between H6 and S4, "dr-C*" for residues Leu-253 to Pro-271 in the region of S11 and S12, "dr-D" for residues Arg-369 to Ile-373 between β-strands S16 and S17, "dr-E" for the insertion (CsdB) between Glu-27 and Ile-30 at the end of β-strand S1, "dr-F" for the loops found in CsdB and C-DES between Asp-153 and Glu-157 between β-strand S5 and helix H8, "dr-G" for the insertion (C-DES) between residues Glu-193 and Ala-196 between helix H9 and β-strand S8. The ribbon drawing was prepared in Swiss-PdbViewer rendered with Pov-Ray.

and H5 and thus including H4, extends into the active site and contributes residues Ile-61, Trp-64, and Trp-69 that are important in monomer−monomer contacts and may be involved in substrate recognition. CsdB has a more extended loop between strand A and helix 3 that kynureninase lacks. Region dr-C* provides conserved Trp-256* and well-conserved Phe-257*. Region dr-D of CsdB has a helix missing in C-DES and kynureninase that extends near the active site and directs Cys-362 into the active site of this protein, where it can play a role in catalysis (*22*). The other regions (dr-B, dr-E, dr-F, and dr-G), in addition to being structurally different with respect to CsdB and C-DES, are also very variable across the kynureninases (the regions are also denoted in Figure 2 associated with the corresponding amino acid sequences), suggesting that other kynureninases would have significant conformational differences there that are not important in catalytic function.

Sequence Homology with Other Kynureninases. Sequence alignments of *P. fluorescens* kynureninase with other bacterial and eukaryotic kynureninases show that there is high homology between multiple bacteria and nonplant eukaryotes (Figure 2 and the Supporting Information). No plant species were identified in the PSI-BLAST analysis. The unrooted tree (not shown) clusters the eukaryotic kynureninases (from *S. cerevisiae*, *Neurospora crassa*, *C. elegans*, and *Homo sapiens*) separately from *most* of the bacterial enzymes (from *Pseudomonas*, *Deinococcus*, *Bordatella*, *Ralstonia*, and *Xanthomonas* species, etc). Interestingly, the kynureninases of *Bacillus anthracis* and *Cytophaga hutchinsonii* have higher sequence homology to the higher organisms and may represent recovery of the gene from a host.

One cluster of absolutely conserved residues surrounds the substrate-binding site and defines a pocket around the pyridine ring of the cofactor (Figure 4). Conserved active site residues include Asn-35, Ser-26, Leu-37, Phe-129, Pro-130, Asp-132, Tyr-176, Asp-201, His-204, Cys-224, Tyr-226, Lys-227, Pro-233, Asp-367, Arg-369, and Arg-375. A second shell of residues extends from the active site and defines a set of structurally critical residues that are hydrophobic. These conserved residues are Ile-122, Tyr-134, Trp-200, Gly-207, Leu-213, Tyr-220, Tyr228, Leu-229, Asn230, Trp-240, Leu-295, Phe-298, Pro-335, Gly-342, Pro-371, Leu-381, Tyr-382, and Val-388. Asp-219 (hydrogen bonding to highly conserved His-192) is the lone hydrophilic residue serving to stabilize the packing of helix H9 to helix H10 and β-strand S9. A final set of conserved residues is important in oligomerization. These residues, Leu-37, Trp-56, Trp-69, Pro-233, and Trp-256, lie at the dimer interface. Trp-256 additionally hydrogen bonds to the phosphate oxygen of the cofactor. Interestingly, amino acids surrounding the phosphate of the cofactor are poorly conserved in the sense that serines (Ser-98) and threonines (Thr-96, -97, -131, and -282*) are randomly substituted among the kynureninases.

Several additional amino acids in the kynureninases are conserved as compensating double mutations. The volume of Trp-64 and neighboring Thr-282 in the bacterial kynureninases is largely matched with a histidine/asparagine pair in the eukaryotes. Another compensating mutation set is the Gly-223 and Phe-238 (or Tyr/Ile) pair shifting to tryptophan and glycine. In this case, most bacteria use Gly at 223, with the interesting exceptions of *B. anthracis* and *C. hutchinsonii*.

Active Site. A schematic picture of the residues associated with the pyridoxal-5′-phosphate cofactor is shown in Figure 5. Phe-129 is π-stacked atop the pyridine ring of the PLP cofactor. There is a hydrogen bond between the internal aldimine NH and the 3′-O of the PLP, with an N−O distance of 2.68 Å. This is consistent with the spectroscopic properties of kynureninase, which shows an absorption maximum at 423 nm (*37*) that indicates a preference for a ketoenamine structure for the internal aldimine. In addition, the Nϵ of His-204 is 3.85 Å from the 3′-O of PLP. His-204 is strictly conserved in all known sequences of kynureninase. Although the distance from His-204 to the 3′-O of PLP (3.85 Å) and the geometry are not conducive to hydrogen bonding in the internal aldimine, His-204 could interact with the 3′-O during catalysis. The structure shows the conserved Asp-201 in the PLP-binding site, which is expected for a member of the aminotransferase family of PLP-dependent enzymes (*12*). In addition, the structure has an additional strictly conserved

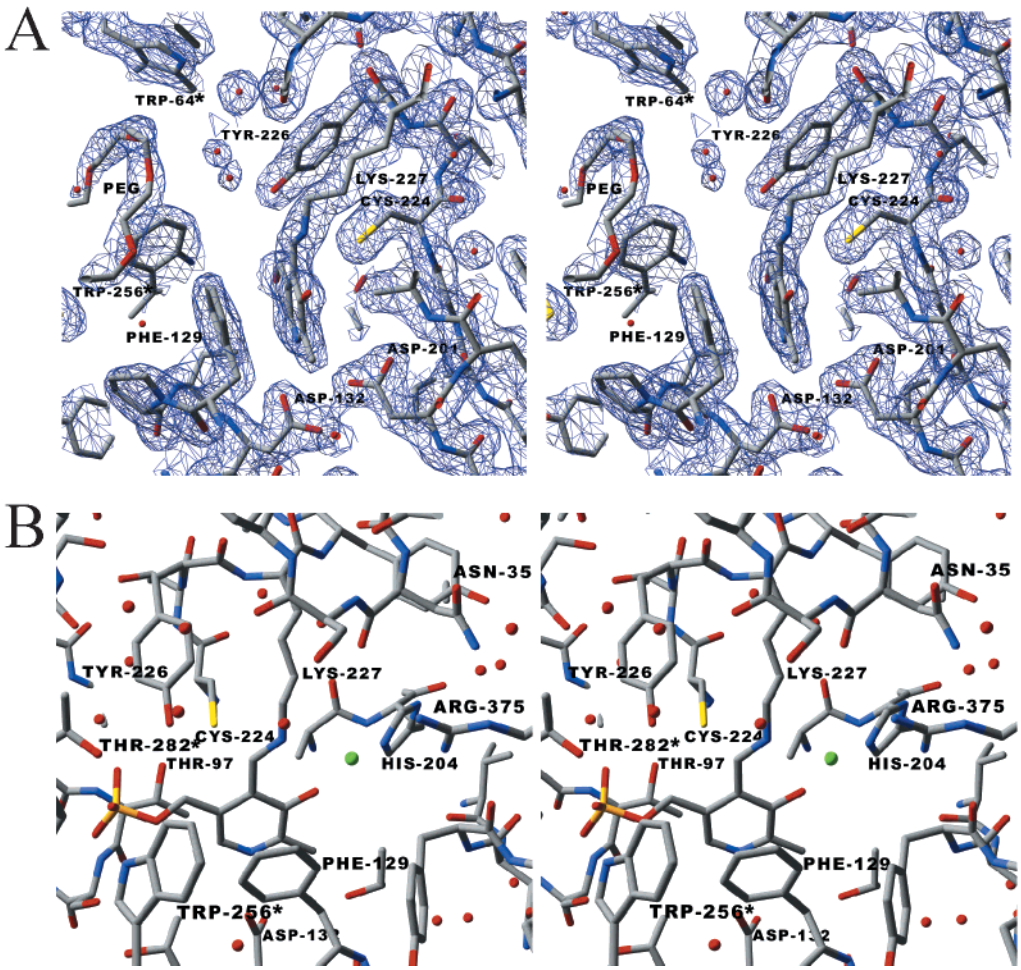

FIGURE 4: Stereoview of the active site region around the pyridoxal-5′-phosphate. Panel A illustrates representative electron density contoured at 1.2σ (SigmaA weighted $2F_o-F_c$) around the PLP cofactor. Only a thin slab of density and atoms is shown for clarity. Note the continuous density between Lys-227 and the cofactor and the well-defined density around aspartates 132 and 201. Extraneous density modeled as a polyethylene glycol polymer is visible on the left-hand side of the cofactor. Panel B represents a view looking at the cofactor roughly from the bulk solvent. Residues from the 2-fold symmetry related monomer are denoted with an asterisk.

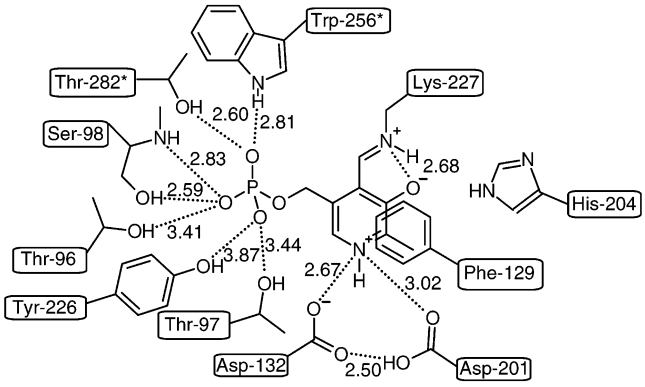

FIGURE 5: Schematic representation of residues interacting with the PLP. Distances between potential hydrogen-bonding partners are indicated in angstroms.

aspartate, Asp-132, which is located at a similar distance from the PLP nitrogen (Figure 5). There is significant electron density located between Asp-132 and Asp-201, and the distance between Oδ of Asp-132 and Oδ of Asp-201 is 2.50 Å, indicating that a hydrogen bond is likely between the two aspartates. The short distance between the two aspartates suggests that there may be a low-barrier hydrogen bond (*38*).

The phosphate oxygens are surrounded by a variety of hydrogen bond donors. Trp-256* and Thr-282* from the other chain of the dimer donate hydrogen bonds to one of the oxygens. The Nα-H and the Oγ of Ser-98 are located in hydrogen-bonding distance from another phosphate oxygen, as is the Oγ of Thr-96. Tyr-226 and Thr-97 provide hydrogen bonds to the third phosphate oxygen. Of the residues involved in phosphate binding, only Tyr-226 and Trp-256 are strictly conserved. While many PLP-dependent enzymes stabilize the phosphate charge via an ionic interaction, for instance using a histidine (CsdB, C-DES, and even the distantly related ornithine decarboxylase), kynureninase has no basic residues nearby to provide this charge stabilization. Like other aminotransferase-like enzymes, a helix dipole from α-helix H6 is appropriately oriented to provide some charge stabilization.

An atom, most likely a chloride ion, sits in the active site where the carboxyl group of the substrate would normally interact. This is similar to the acetate ion found in the structures of the related enzymes C-DES and CsdB. Assignment of the atom as a chloride ion was made on the basis of the strong anomalous signal of this ion, its presence in the crystallization buffer, and the strong electron density.

One further feature of the kynureninase structure is the presence of extraneous electron density near the active site

Table 3: PLP Binding Constants and Activity of Wild-Type and Mutant Kynureninase

enzyme	K_d, PLP, nM	k_{cat}/K_m, kynurenine, M^{-1} s^{-1}
wild type	628 ± 35	6.3×10^5
D132E	128 ± 14	2.1×10^5
D132A	5100 ± 590	7.4×10^4
D201E	15.1 ± 1.5	2.3×10^4
D201A	7010 ± 2300	20

(Figure 4). Since the crystals were prepared in low molecular weight polyethylene glycol, it may be a tightly bound molecule of PEG. Alternatively, it could be a fatty acid maintained through purification. The uncharacterized molecule actually occupies the same region as an extra loop (12 additional amino acids) found in CsdB (Thr-360 to Met-377 of CsdB, which corresponds to region dr-D, Figure 3) that is absent in the kynureninases. The eukaryotic, as well as *B. anthracis* and *C. hutchinsonii*, kynureninases have small insertions of two additional amino acids in this region. Many of the residues surrounding the putative PEG molecule are conserved, so this may have biological implications and certainly offers an extra handle for drug design. One further important point to make related to this extraneous feature is that this molecule may be occupying a site normally filled by residues His-259* through Glu-266* of kynureninase (region dr-C*). This loop was difficult to trace because of poor electron density. Phe-263* is located in the middle of this loop and has very poor side-chain electron density. This is quite surprising and was cause for alarm during initial model building because it is absolutely conserved. The explanation for the poor side-chain electron density of an absolutely conserved residue could be that the loop normally is associated with the active site, and that it has been displaced in the crystal structure by a crystallization reagent, PEG.

Mutagenesis of Asp-132 and Asp-201. We prepared the Ala and Glu mutants of Asp-132 and Asp-201 by site-directed mutagenesis to probe their roles in PLP binding and catalysis. Surprisingly, both D132E and D201E kynureninases have good activity and PLP binding stronger than that of the wild-type enzyme (Table 3). However, D132A kynureninase has lower activity and binds PLP weakly (Table 3). D201A kynureninase has very low activity, less than 0.01% of that of the wild-type enzyme, binds PLP weakly, and expresses poorly, giving large amounts of insoluble inclusion bodies and very low levels of soluble protein. This is expected, since Asp-201 is homologous to the conserved PLP-binding aspartate found in all members of the aminotransferase family (*12*).

DISCUSSION

Kynureninase is an enzyme in tryptophan catabolism that is inducible in bacteria such as *P. fluorescens*, but which is constitutive in eukaryotes (*1*). However, *N. crassa* was reported to have both inducible and constitutive kynureninases (*39*). The inducible kynureninase reacts with L-kynurenine, while the constitutive enzyme reacts preferentially with 3-hydroxy-L-kynurenine (*1*). The constitutive kynureninase plays a key role in the pathway for de novo synthesis of $NAD(P)^+$ in eukaryotes. There is homology, and significant identity, in all known kynureninase sequences, from bacteria to man (Figure 2). Thus, both inducible and constitutive kynureninases must have a similar fold and three-dimensional structure. We note that the majority of the conserved residues in Figure 2 are located in or very near the PLP-binding site. The structure confirms the prediction from sequence alignment that Lys-227 is the PLP-binding residue in *P. fluorescens* kynureninase.

Sequence alignment of kynureninase with other PLP-dependent enzymes shows that kynureninase is in subgroup IVa of the aminotransferases, along with nifS, CsdB, and serine-pyruvate aminotransferase (*12*). Indeed, the coordinates of CsdB were used for molecular replacement in the solution of the structure of kynureninase, after molecular replacement failed with both aspartate aminotransferase and tyrosine phenol-lyase coordinates. It is interesting to note that all of the members of subgroup IVa share similar reaction characteristics, in that they catalyze either β-elimination reactions with electrophilic replacement or transamination, resulting in L-alanine as a product.

All PLP-dependent enzymes in the aminotransferase family have an aspartate residue in close contact with the PLP pyridine N1, to keep it protonated to enhance the electrophilicity of the cofactor (*12*). The sequence alignment predicts that Asp-201, which is strictly conserved in kynureninases, is the corresponding residue in *P. fluorescens* kynureninase. We do observe in the structure that Asp-201 is near the PLP nitrogen, but in addition, we find that Asp-132 is also at a similar distance and is also strictly conserved. The results show that both residues contribute to PLP binding, but Asp-201 has a much greater contribution to activity. Tyr-226 is the residue just preceding the PLP-binding lysine, and this residue is strictly conserved in kynureninases, although tyrosine is not found in this position in any other PLP-dependent enzyme. The structure shows that Tyr-226 donates a hydrogen bond to the phosphate of the PLP. However, it is not uncommon for aminotransferases to have a tyrosine involved in PLP binding. In aspartate aminotransferase, Tyr-70 donates a hydrogen bond to the phosphate of PLP, and serves mainly to bind PLP (*40*). In the case of tyrosine phenol-lyase, Tyr-71 donates a hydrogen bond to the PLP phosphate in the internal aldimine, but also is a general acid for the elimination step of the reaction (*41*). Trp-256, which is strictly conserved in kynureninases, also donates a hydrogen bond to the phosphate through the indole N1 hydrogen. To our knowledge, the participation of a tryptophan residue in PLP binding through the phosphate is unique to kynureninase and C-DES. Finally, the strictly conserved Phe-129 is π-stacked on the pyridine ring of PLP. This is also commonly observed in aminotransferase family members.

We have studied the mechanism of kynureninase previously using both steady-state (*42*) and pre-steady-state kinetic techniques (*37*). The pH dependence of k_{cat}/K_m showed that there is only a single catalytic base, with a pK_a of 6.25, required for multiple proton transfers during the reaction (*42*). The most likely residue for the base is Lys-227, since it requires a great deal of dexterity. The catalytic base must remove the proton from the α-carbon of the kynurenine external aldimine (EA_1) and then protonate C-4′ of the quinonoid intermediate (EQ_1) (Scheme 1). It then assists water in addition to the γ-carbonyl of the ketimine intermediate (EK_1) to form the *gem*-diolate (ED), protonates the

β-carbon of the enamine (EE), and finally shuttles the proton from C-4′ of the pyruvate ketimine (EK_2) back to Cα to give the alanine external aldimine (EA_2). The sequence alignment of kynureninase with the other members of the aminotransferase family shows a conserved arginine residue, Arg-375, which is homologous to the substrate α-carboxylate-binding site in other members of the family. In our structure, the carboxylate of L-alanine can be docked with Arg-375 with the amino group oriented toward the PLP Lys-227 Schiff base to undergo external aldimine formation (data not shown). Thus, our results confirm that Arg-375 is a substrate-binding residue. In the present structure, the putative α-carboxylate-binding site is occupied by a sphere of electron density, probably a chloride ion, which provides confirmation that it is an anion-binding site.

The structure of *P. fluorescens* kynureninase reported herein provides information essential for the future testing of the role of active site residues in the mechanism of the reaction using site-directed mutagenesis. In addition, the homology with eukaryotic, especially human (28% identity), kynureninases will allow for the convenient structure determination in the future using the molecular replacement method. The structure of human kynureninase will help in the design of novel, potent, and specific inhibitors, which may be of value as CNS active drugs.

ACKNOWLEDGMENT

We thank Drs. Nobuyoshi Esaki and Yasuo Hata for the generous use of the CsdB coordinates before publication.

SUPPORTING INFORMATION AVAILABLE

Multiple sequence alignment (CLUSTAL-W) of kynureninases in PDF format. Coordinates are available from the Protein Data Bank, ID code **1QZ9**. This material is available free of charge via the Internet at http://pubs.acs.org.

REFERENCES

1. Soda, K., and Tanizawa, K. (1979) Kynureninases: enzymological properties and regulation mechanism, *Adv. Enzymol. Relat. Areas Mol. Biol. 49*, 1−40.
2. Birley, S., Collins, J. F., Perkins, M. N., and Stone, T. W. (1982) The effects of cyclic dicarboxylic acids on spontaneous and amino acid- evoked activity of rat cortical neurones, *Br. J. Pharmacol. 77*, 7−12.
3. Saito, K., Crowley, J. S., Markey, S. P., and Heyes, M. P. (1993) A mechanism for increased quinolinic acid formation following acute systemic immune stimulation, *J. Biol. Chem. 268*, 15496−15503.
4. Sei, S., Saito, K., Stewart, S. K., Crowley, J. S., Brouwers, P., Kleiner, D. E., Katz, D. A., Pizzo, P. A., and Heyes, M. P. (1995) Increased human immunodeficiency virus (HIV) type 1 DNA content and quinolinic acid concentration in brain tissues from patients with HIV encephalopathy, *J. Infect. Dis. 172*, 638−647.
5. Sei, Y., Paul, I. A., Saito, K., Layar, R., Hartley, J. W., Morse, H. C., 3rd, Skolnick, P., and Heyes, M. P. (1996) Quinolinic acid levels in a murine retrovirus-induced immunodeficiency syndrome, *J. Neurochem. 66*, 296−302.
6. Saito, K., Nowak, T. S., Jr., Markey, S. P., and Heyes, M. P. (1993) Mechanism of delayed increases in kynurenine pathway metabolism in damaged brain regions following transient cerebral ischemia, *J. Neurochem. 60*, 180−192.
7. Saito, K., Nowak, T. S., Jr., Suyama, K., Quearry, B. J., Saito, M., Crowley, J. S., Markey, S. P., and Heyes, M. P. (1993) Kynurenine pathway enzymes in brain: responses to ischemic brain injury versus systemic immune activation, *J. Neurochem. 61*, 2061−2070.
8. Heyes, M. P., Brew, B., Martin, A., Markey, S. P., Price, R. W., Bhalla, R. B., and Salazar, A. (1991) Cerebrospinal fluid quinolinic acid concentrations are increased in acquired immune deficiency syndrome, *Adv. Exp. Med. Biol. 294*, 687−690.
9. Heyes, M. P., Swartz, K. J., Markey, S. P., and Beal, M. F. (1991) Regional brain and cerebrospinal fluid quinolinic acid concentrations in Huntington's disease, *Neurosci. Lett. 122*, 265−269.
10. Achim, C. L., Heyes, M. P., and Wiley, C. A. (1993) Quantitation of human immunodeficiency virus, immune activation factors, and quinolinic acid in AIDS brains, *J. Clin. Invest. 91*, 2769−2775.
11. Koushik, S. V., Sundararaju, B., McGraw, R. A., and Phillips, R. S. (1997) Cloning, Sequence and Expression of Kynureninase from *Pseudomonas fluorescens*, *Arch. Biochem. Biophys. 344*, 301−308.
12. Alexander, F. W., Sandmeier, E., Mehta, P. K., and Christen, P. (1994) Evolutionary relationships among pyridoxal-5′-phosphate-dependent enzymes. Regio-specific alpha, beta and gamma families, *Eur. J. Biochem. 219*, 953−960.
13. Bose, N., Greenspan, P., and Momany, C. (2002) Expression of recombinant human betaine: homocysteine S-methyltransferase for x-ray crystallographic studies and further characterization of interaction with S-adenosylmethionine, *Protein Expr. Purif. 25*, 73−80.
14. Moriguchi, M., Yamamoto, T., and Soda, K. (1971) Inactivation of kynureninase by L-alanine, *Biochem. Biophys. Res. Commun. 44*, 1416−1419.
15. Davies, D. R., and Segal, D. M. (1972) Protein crystallization: micro techniques involving vapor diffusion, *Methods Enzymol.* 266−269.
16. McPherson, A. (1976) Crystallization of proteins from polyethylene glycol, *J. Biol. Chem. 251*, 6300−6303.
17. Jancarik, J., and Kim, S. H. (1991) Sparse matrix sampling: a screening method for crystallization of proteins, *J. Appl. Crystallogr. 24*, 409−411.
18. Dauter, Z., Dauter, M., and Rajashankar, K. R. (2000) Novel approach to phasing proteins: derivatization by short cryo-soaking with halides, *Acta Crystallogr. D56*, 232−237.
19. Otwinowski, Z. (1993) Denzo, in *Data Collection and Processing* (Sawyer, L., Isaacs, N., and Bailey, S., Eds.) pp 56−62, SERC Daresbury Laboratory, Warrington, U.K.
20. Otwinowski, Z., and Minor, W. (1997) Processing of X-Ray Diffraction Data Collected in Oscillation Mode, *Methods Enzymol. 276*, 307−326.
21. Terwilliger, T. C., and Berendzen, J. (1999) Automated MAD and MIR structure solution, *Acta Crystallogr. D55*, 849−861.
22. Fujii, T., Maeda, M., Mihara, H., Kurihara, T., Esaki, N., and Hata, Y. (2000) Structure of a NifS homologue: X-ray structure analysis of CsdB, an *Escherichia coli* counterpart of mammalian selenocysteine lyase, *Biochemistry 39*, 1263−1273.
23. Mihara, H., Maeda, M., Fujii, T., Kurihara, T., Hata, Y., and Esaki, N. (1999) A *nifS*-like Gene, *csdB*, Encodes an *Escherichia coli* Counterpart of Mammalian Selenocysteine Lyase. Gene Cloning, Purification, Characterization And Preliminary X-Ray Crystallographic Studies, *J. Biol. Chem. 274*, 14768−14772.
24. Navaza, J. (1994) AMoRE: an automated package for molecular replacement, *Acta Crystallogr. D50*, 157−163.
25. Otwinowski, Z. (1991) Isomorphous replacement and anomalous scattering, in *Proceedings of the CCP4 Study Weekend* (Wolf, W., Evans, P. R., and Leslie, G. W., Eds.) pp 80−86, SERC Daresbury Laboratory, Warrington, U.K.
26. CCP4, Collaborative Computational Project, Number 4 (1994) The CCP4 Suite: programs for protein, *Acta Crystallogr. D50*, 760−763.
27. Cowtan, K., and Main, P. (1998) Miscellaneous algorithms for density modification, *Acta Crystallogr. D54*, 487−493.
28. Jones, T. A., Zou, J. Y., Cowan, S. W., and Kjeldgaard. (1991) Improved methods for binding protein models in electron density maps and the location of errors in these models, *Acta Crystallogr. A47*, 110−119.
29. Murshudov, G. N., Vagin, A. A., and Dodson, E. J. (1997) Refinement of macromolecular structures by the maximum-likelihood method, *Acta Crystallogr. D53*, 240−255.
30. Lamzin, V. S., and Wilson, K. S. (1993) Automated refinement of protein models, *Acta Crystallogr. D49*, 129−147.
31. Lovell, S. C., Davis, I. W., Arendall, W. B., 3rd, de Bakker, P. I., Word, J. M., Prisant, M. G., Richardson, J. S., and Richardson, D. C. (2003) Structure validation by Calpha geometry: phi,psi and Cbeta deviation, *Proteins 50*, 437−450.

32. Cleland, W. W. (1979) Statistical analysis of enzyme kinetic data, *Methods Enzymol. 63*, 103−138.
33. Altschul, S. F., Madden, T. L., Schaffer, A. A., Zhang, J., Zhang, Z., Miller, W., and Lipman, D. J. (1997) Gapped BLAST and PSI−BLAST: a new generation of protein database search programs, *Nucleic Acids Res. 25*, 3389−3402.
34. Thompson, J. D., Higgins, D. G., and Gibson, T. J. (1994) CLUSTAL W: improving the sensitivity of progressive multiple sequence alignment through sequence weighting, position-specific gap penalties and weight matrix choice, *Nucleic Acids Res. 22*, 4673−4680.
35. Shine, J., and Dalgarno, L. (1974) The 3′-terminal sequence of *Escherichia coli* 16S ribosomal RNA: complementarity to nonsense triplets and ribosome binding sites, *Proc. Natl. Acad. Sci. U.S.A. 71*, 1342−1346.
36. Jansonius, J. N. (1998) Structure, evolution and action of vitamin B6-dependent enzymes, *Curr. Opin. Struct. Biol. 8*, 759−769.
37. Phillips, R. S., Sundararaju, B., and Koushik, S. V. (1998) The Catalytic Mechanism of Kynureninase from *Pseudomonas fluorescens*: Evidence for Transient Quinonoid and Ketimine Intermediates from Rapid-scanning Stopped-flow Spectrophotometry, *Biochemistry 37*, 8783−8789.
38. Cleland, W. W., and Kreevoy, M. M. (1994) Low-barrier hydrogen bonds and enzymic catalysis, *Science 264*, 1887−1890.
39. Gaertner, F. H., Cole, K. W., and Welch, G. R. (1971) Evidence for distinct kynureninase and hydroxykynureninase activities in *Neurospora crassa*, *J. Bacteriol. 108*, 902−909.
40. Toney, M. D., and Kirsch, J. F. (1987) Tyrosine 70 increases the coenzyme affinity of aspartate aminotransferase. A site-directed mutagenesis study, *J. Biol. Chem. 262*, 12403−12405.
41. Chen, H. Y., Demidkina, T. V., and Phillips, R. S. (1995) Site-directed mutagenesis of tyrosine-71 to phenylalanine in *Citrobacter freundii* tyrosine phenol-lyase: evidence for dual roles of tyrosine-71 as a general acid catalyst in the reaction mechanism and in cofactor binding, *Biochemistry 34*, 12276−12283.
42. Koushik, S. V., Moore, J. A., 3rd, Sundararaju, B., and Phillips, R. S. (1998) The Catalytic Mechanism of Kynureninase from *Pseudomonas fluorescens*: Insights from the Effects of pH and Isotopic Substitution on Steady State and Pre-steady-State Kinetics, *Biochemistry 37*, 1376−1382.
43. Guex, N., and Peitsch, M. C. (1997) SWISS-MODEL and the Swiss-PdbViewer: an environment for comparative protein modeling, *Electrophoresis 18*, 2714−2723.

BI035744E